Oil Shale, 2014, Vol. 31, No. 2, pp. 105–120
doi: 10.3176/oil.2014.2.02
ISSN 0208-189X

TEMPERATURE DISTRIBUTION SIMULATION AND OPTIMIZATION DESIGN OF ELECTRIC HEATER FOR IN-SITU OIL SHALE HEATING

YANG HAO*, GAO XIAOQIAO, XIONG FANSHENG, ZHANG JIALIANG, LI YANJU

Key Laboratory on Deep GeoDrilling Technology of the Ministry of Land and Resources, China University of Geosciences (Beijing), Beijing, 100083, China

Abstract. *Electric heating is the main method of exploiting oil shale and electric heater is the key part of the heating element. In this paper, the temperature distribution of the electric heater was simulated by the Partial Differential Equation (PDE) of MATLAB, and orthogonal experiment analysis was also carried out to investigate the effects of different factors on the temperature distribution of the heater. The results showed that materials with low density were helpful to improve heating efficiency, and heat production, density and heat capacity had a great effect on the temperature distribution of the heater. The temperature distribution of the heater increased significantly with increasing heat production and radius of the heater, while higher heat capacity always led to the lower overall temperature of the heater. In addition, axisymmetric U-tube and vacuum heating tube were chosen as the heater, being of optimized shape, while copper and stainless steel were determined to be the optimized heater materials.*

Keywords: *oil shale, in-situ treatment, electric heater, PDE, optimization design*.

1. Introduction

Oil shale is a source of energy with great potential that has been internationally recognized as one of the most important substitutes for conventional oil resources [1–2]. There are two kinds of conventional methods for mining oil shale – opencast and underground [3]. Both the mining methods, however, have drawbacks. Opencast mining occupies much land and causes environmental pollution. Underground mining takes up much land, too, because the produced ore must be accumulated on the ground. Moreover, the

* Corresponding author: e-mail *yanghao@cugb.edu.cn*

groundwater level under the oil shale layers may be lowered, which jeopardizes the water regime of arable lands and forests near the mines.

The in-situ conversion treatment technology by subterranean thermal conductivity consists in drilling heater wells in formations containing oil shale and then heating the oil shale layers directly, which converts hydrogen-rich compounds from liquids into gaseous state by enrichment and phase changes of tight carbon components [4]. Then, these lighter hydrocarbons flow into the nearby production wellbore zone through natural cracks or artificial fractures underground, the recovery of underground crude carbons can be up to 65–70%. According to heating source, the in-situ conversion treatment technology can be grouped into IVE technology (hot gas heating) and ICP technology (electric heating). The IVE technology wastes much valuable natural gas resource and requires constructing a gas line. Also, when injecting hot gas stream, the drawback is that the injection equipment occupies too much land. Even more, the pyrolysis temperature of oil shale may range from 350 to 560 °C, but the injected gas stream cannot attain these temperatures because of thermal loss. Compared with the IVE technology, the heating mode and construction process of the ICP technology are simpler and the thermal efficiency is higher. Moreover, the heater temperature can be up to 1000 °C, which is adjustable depending on demand. Therefore, electric heating is the optimal method for oil shale development. There can be found papers in the literature, which deal with in-situ oil shale heater [5–14]. But to have more information, the current paper simulated the temperature distribution of in-situ oil shale electric heater and further analyzed the influencing factors. Based on these, an optimized design of the heater was proposed and the heater materials were also determined.

2. Temperature distribution simulation of electric heater

2.1. Physical model of electric heater [15]

Figure 1 shows the schematic diagram of electric heating well. There are sections for export of different kinds of energy along the electric heater. Every section contains a temperature-limiting element to limit energy export, which can provide different quantities of heat at varying heating rates. The electric heating well consists of the following main parts: (1) lead-in conductor, which is used to introduce electrical energy with a service temperature of about 40–60 °C; (2) cold lead, which is used to fully lower the temperature of the heater; (3) connections, which are used to connect cold lead with the heater with a service temperature of 260–370 °C; and (4) heater, which is used to produce heat to reach the temperature of 530–760 °C. Figure 2 presents a simplified schematic diagram of the heater for numerical simulation.

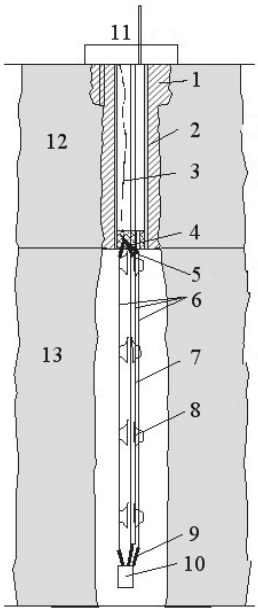

Fig. 1. Schematic diagram of electric heating well: 1 – cement sheath; 2 – casing; 3 – lead-in conductor; 4 – cold lead; 5 – connections; 6 – heater; 7 – supporting part; 8 – plummet; 9 – cold lead; 10 – conductor jointer; 11 – well-head; 12 – overburden; 13 – oil shale layer.

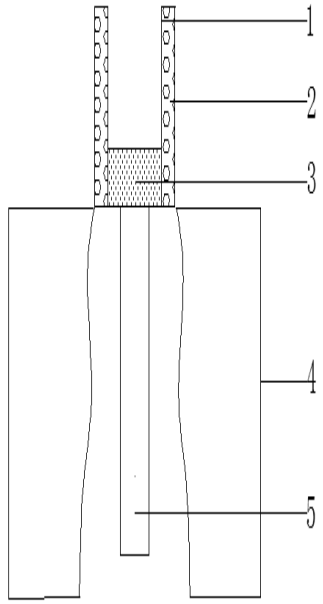

Fig. 2. Simplified schematic diagram of electric heating well: 1 – casing; 2 – cement sheath; 3 – insulating separator; 4 – oil shale layers; 5 – heater.

2.2. Mathematical model of electric heater

Considering the symmetry of wells, the electric heater was designed as a single cylinder to generate uniform heat inside the wells. The initial temperature of the heater was the formation temperature at the corresponding depth. The upper end of the heater was adiabatic, while the bottom end could convect with the borehole fluid. In order to reflect the radial and axial temperature distribution of the heater, a cylindrical coordinate system (r, θ, z) was adopted. Meanwhile, considering the symmetry of electric heater (i.e. independence of θ), a parabolic equation was adopted to solve the heat conduction temperature field problem of pillar-shaped objects, and the basic equation could be expressed as follows:

$$r\rho c_p \frac{\partial u}{\partial t} - \frac{\partial}{\partial r}\left(kr\frac{\partial u}{\partial r}\right) - \frac{\partial}{\partial z}\left(kr\frac{\partial u}{\partial r}\right) = q_v r\,, \tag{1}$$

where ρ is density, kg/m^3; c_p is heat capacity, $J/(kg\cdot K)$; k is the coefficient of thermal conductivity, $W/(\mathrm{m}\cdot K)$; q_v is heat production, kW/m^3; r is

radical radius, m; and z is the length of heater, m. The boundary conditions are as follows:

$$\begin{cases} hu = r \\ n \cdot (c\nabla u) + qu = g, \end{cases} \tag{2}$$

where n is a unit vector perpendicular to the boundaries, and h, r, q and g are constants or variables related to u. The first equation of equation group (2) is called Dirichlet Boundary Condition, and the second is called Neumann Boundary Condition. In the thermal conductivity field, the first boundary condition corresponds to the Dirichlet Boundary Condition, and the second and third correspond to the Neumann Boundary Condition. The corresponding relationship can be realized by the PDE toolbox of MATLAB.

3. Numerical simulation of the heater temperature field by MATLAB

3.1. Assumed conditions

Prior to numerical simulation, the following assumptions can be made:

(1) The electric heater is located in the center of the well.
(2) Physical conditions are consistent around the well.
(3) Physical parameters are stable and not altered with temperature.

3.2. Calculation parameters

The PDE Toolbox GUI of MATLAB was used to simulate the temperature distribution of heater 5 depicted in Figure 2. The heater was a metal rod with a bare electrode, with density ρ of 7800 kg/m^3, heat capacity c_p of 500 J/kg·°C, thermal conductivity k of 40 W/m·°C and heat production q_v of 750 kW/m^3. The coefficient of convective heat transfer (λ) between water and the bottom or side of the heater was 50 W/m^2·°C, and the upper end of the heater was adiabatic.

3.3. Numerical simulation of the temperature distribution of heater

Figures 3 and 4 demonstrate that the temperature of the upper end of heater is higher because it is adiabatic, while that of the bottom end is lower due to heat convection. Meanwhile, because of the axial symmetry of the heater, the temperature distribution is symmetrical. Therefore, the numerical simulation reflects the actual temperature distribution of the heater.

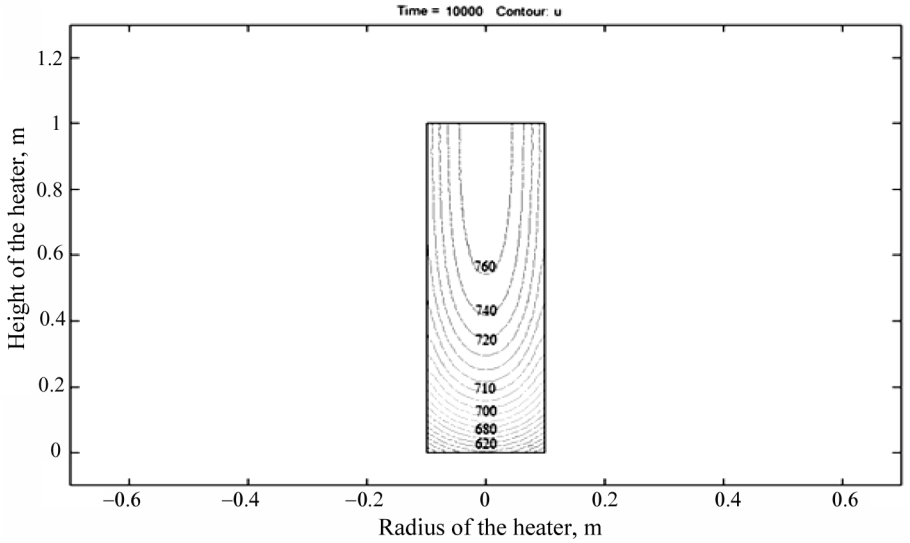

Fig. 3. 2-D temperature field at 10 000 s.

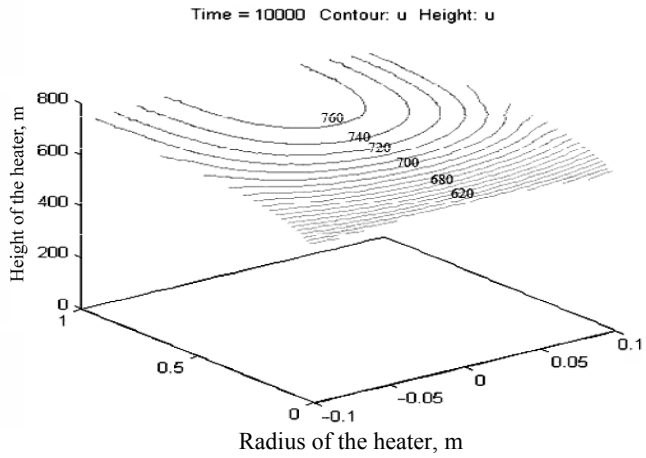

Fig. 4. 3-D temperature field profile at 10 000 s.

4. Optimization of electric heater design

4.1. Factors influencing the parameters of electric heater

The results of simulation are affected by many parameters of the heater, including thermal conductivity, heat production, density, heat capacity, size, etc. This work provides references for the optimization design of electric heater by analyzing the effects of these parameters on the heater temperature distribution. The simulation data were obtained, considering density, thermal conductivity, heat capacity, heat source density or the radius of heater as a single variable. The temperature values of the heater at 10 000 s were

recorded, t_{max} designating the highest temperature, t_{min} the lowest temperature, T_a the average temperature and T_d representing the difference between maximum and minimum temperatures.

4.1.1. Density

Figure 5 shows the temperature distribution of the heater at different densities. It can be seen that the temperature of the whole heater increases as the density decreases. Low-density materials are beneficial to improve the heat efficiency of the heater, while those with high density go against the balanced distribution of temperature.

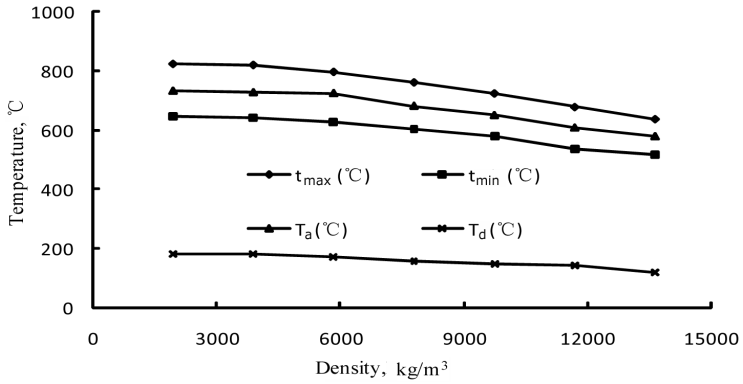

Fig. 5. Temperature distribution at different densities.

4.1.2. Thermal conductivity

As shown in Figure 6, the temperature varies little as thermal conductivity increases, but high thermal conductivity is beneficial to balance temperature distribution.

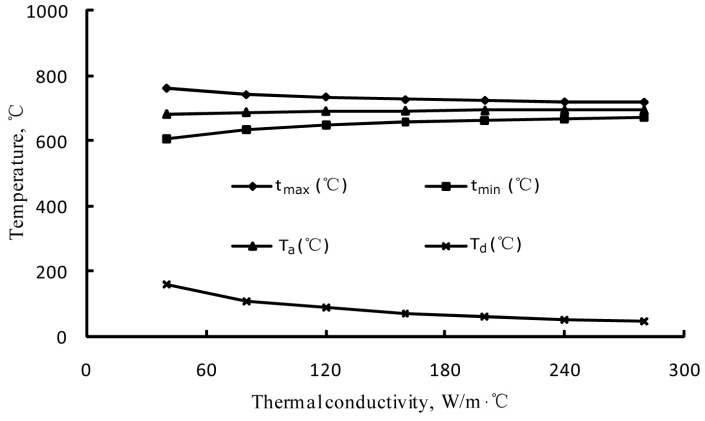

Fig. 6. Temperature distribution at different thermal conductivities.

4.1.3. Heat capacity

As the heat capacity of the materials increases, the temperature decreases, but high heat capacity is beneficial to the balanced distribution of temperature, as shown in Figure 7.

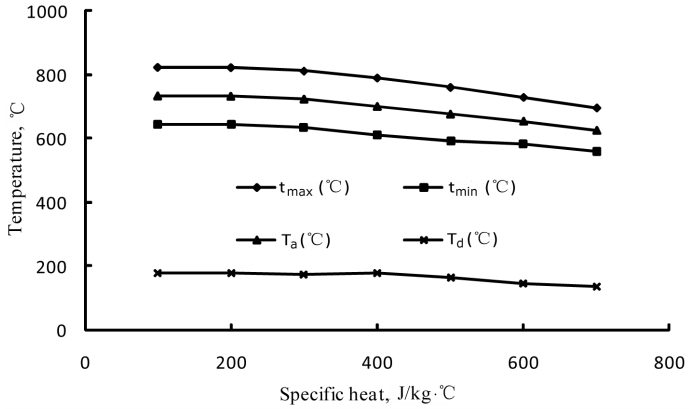

Fig. 7. Temperature distribution at different heat capacities.

4.1.4. Heat production

As Figure 8 shows, the temperature of the heater increases significantly with increasing heat production. Heat production is the ratio of power to volume, and the increase of heat production means the increase of power, which may lead to an obvious increase of the temperature. Meanwhile, the increase of power may also cause an increase of the imbalance of heat temperature distribution.

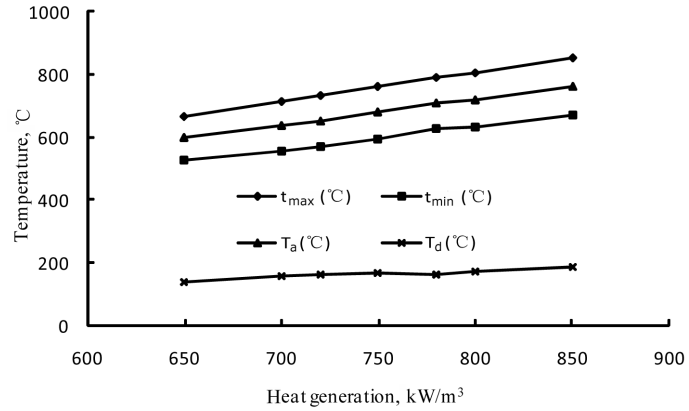

Fig. 8. Temperature distribution at different heat source densities.

4.2. Analysis of the effect of physical parameters

Orthogonal experiment was used to analyze the effect of physical parameters on temperature distribution. Through model derivation and numerical simulation, the following four factors were selected (as shown in Table 1): density (factor A), thermal conductivity (factor B), heat capacity (factor C) and heat production (factor D). Taking the maximum temperature as an index, a four-factor three-level orthogonal experiment was conducted on heater temperature distribution. The results are presented in Table 2. According to the R_j values, D > A > C > B, i.e. the index of factor D fluctuates maximally and that of factor B fluctuates minimally. Therefore, heat production, density and heat capacity should be mainly considered when designing electric heater.

Table 1. Factors and levels of orthogonal experiment

Level	Factors			
	A (density), kg/m^3	B (thermal conductivity), W/(m·K)	C (heat capacity), J/(kg·K)	D (general heat), kW/m^3
1	3900	40	300	700
2	7800	120	500	750
3	11700	200	700	800

Table 2. Orthogonal experiment results

Experiment number	A	B	C	D	Maximum temperature, °C
1	1	1	1	1	752
2	1	2	2	2	781
3	1	3	3	3	806
4	2	1	2	3	813
5	2	2	3	1	628
6	2	3	1	2	766
7	3	1	3	2	586
8	3	2	1	3	793
9	3	3	2	1	608
I_j	2339	2151	2311	1988	
II_j	2207	2202	2202	2133	
III_j	1987	2180	2020	2412	
R_j	352	51	291	424	

Notes: the results of nine experiments are divided into three groups. I_1, II_1 and III_1 represent respectively level-1, level-2 and level-3 of the first column (factor A); R_1 represents the range of I_1, II_1 and III_1; for other columns, I_j, II_j, III_j and R_j represent the same meaning.

4.3. Optimization design of the heater shape

4.3.1. Theoretical analysis

Keeping the voltage constant, heat production q_v can be derived from power and resistivity formulae:

Heater surface area: $$S = \pi r^2 + 2\pi rL, \tag{3}$$

Heater volume: $$V = \pi r^2 L, \tag{4}$$

Power: $$P = \frac{U^2}{R}, \tag{5}$$

Resistance: $$R = eL/S, \tag{6}$$

where S, V, P and R are the heater surface area, heater volume, power and resistance, respectively, U is the voltage, r is the radius of the heater, and L is the height of the heater.

When heating resistances are similar, then:

$$P = \frac{U^2}{R} = U^2 \cdot \frac{R_2R_3\cdots R_{n-1}R_n + R_1R_3\cdots R_{n-1}R_n + R_1R_2\cdots R_{n-1}R_n + \cdots R_1R_2R_3\cdots R_{n-1}}{R_1R_2R_3\cdots R_n}. \tag{7}$$

Putting Equation (6) into Equation (7) will give:

$$P = U^2 \cdot \frac{R_2R_3\cdots R_{n-1}R_n + R_1R_3\cdots R_{n-1}R_n + R_1R_2\cdots R_{n-1}R_n + \cdots R_1R_2R_3\cdots R_{n-1}}{R_1R_2R_3\cdots R_n}$$

$$= U^2 \cdot \frac{n\cdot\left(\frac{eL}{S}\right)^{n-1}}{\left(\frac{eL}{S}\right)^{n}} = nU^2 \cdot \frac{\pi r^2}{eL}. \tag{8}$$

Then, the heat flux q_A can be expressed as:

$$q_A = \frac{P}{A} = nU^2 \cdot \frac{\pi r^2}{eL}\frac{1}{n(\pi r^2 + 2\pi rL)} = \frac{U^2 r}{eL(r+2L)} = \frac{U^2}{eL\left(1+2L/r\right)}, \tag{9}$$

and the heat production rate q_v as:

$$q_v = \frac{P}{V} = nU^2 \cdot \frac{\pi r^2}{eL}\frac{1}{n\pi r^2 L} = \frac{U^2}{eL^2}, \tag{10}$$

where e is resistivity, Ω·m; U is voltage, V; n is the number of heaters; r is the radius of the heater; L is the height of the heater; and A is the area of the

heater. Obviously, as the radius of the heater increases, heat flux increases and heat production rate highly depends on the length of the heater.

4.3.2. Numerical simulation

For numerical simulation parameters were set as follows: density ρ 7800 kg/m^3, heat capacity c_p 500 J/kg·°C, thermal conductivity k 40 W/m·°C, heat production q_v 750 kW/m^3, and length of the heater z 1 m. The coefficient of convective heat transfer (λ) between water and the bottom or side of the heater was 50 W/m^2·°C, as shown in Figure 9. The results of numerical simulation showed that both the temperature and heat flux increased as the radius of the heater increased, and that the temperature differences at different positions of the heater also increased with the increase of heater volume, which conformed well to the theoretical analysis results.

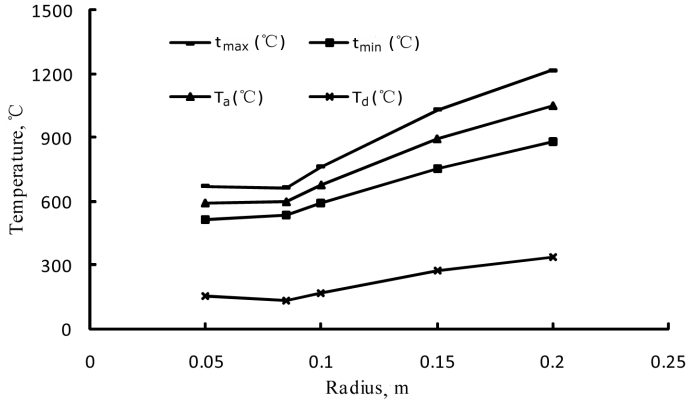

Fig. 9. Temperature distribution at different radii.

4.3.3. Optimization of the heater shape

According to the theoretical analysis, heat production is the reciprocal value of the square of the heater length if the materials of the heater and load voltage remain constant. That is to say, decreasing the length is beneficial to increase the heater temperature, so the minimum length should be the thickness of the oil shale layer. Meanwhile, in order to form a loop, U-tube was adopted as the heater. In consideration of the symmetry of the well, the mutually perpendicular U-tube was finally selected as the heater. Due to the skin effect, the central part of the heater was removed for material saving. Thus, the heater formed a loop between the bottom contractor and its own central part. The annulus of the loop and the heater were evacuated to isolate the high temperature of the heater, so that the cable could work at high temperature. During heating, the heater could coordinate with the injection string and the oil well pump. The schematic diagram of the designed heater is shown in Figures 10 and 11.

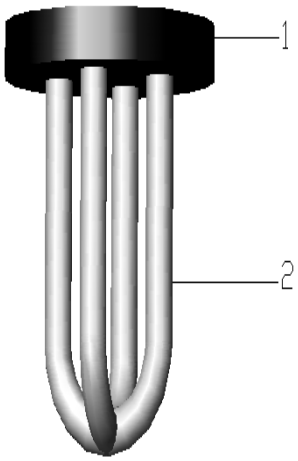

Fig. 10. The axisymmetric U-tube: 1 – insulating separator; 2 – electric heating element.

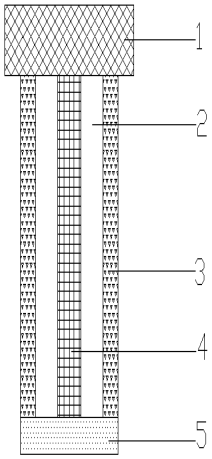

Fig. 11. The vacuum heating tube: 1 – insulating separator; 2 – vacuum insulating separator; 3 – electric heating element; 4 – loop; 5 – contractor.

4.4. Optimization of heating materials

For optimization of heating materials selection was made among iron, copper, aluminum, stainless steel, nichrome, tungsten and graphite. The relevant parameters of these materials are given in Table 3.

Table 3. The characteristic parameters of materials

Parameter	Iron	Copper	Aluminum	Stainless steel	Nichrome	Tungsten	Graphite
Density, g/cm^3	7.9	8.92	2.7	7.7	8.4	19.35	2.2
Heat capacity, kJ/kg·°C	0.46	0.4	0.88	0.5	0.45	0.13	0.71
Thermal conductivity, W/m·°C	46	401	237	30.6	12.3–171	325	129
Resistivity, 10^{-8}Ω·m	9.78	1.75	2.83	40	100	5.65	800–1300
Melting point, °C	1535	1083	660	1430	1400	3410	3652

The heating element of the heater was a cylinder with the radius r of 0.1 m and length of 1 m. The coefficient of convective heat transfer (λ) between the side or bottom of the heater and the fluid on the surface was set at 50 W/m^2·°C. The heat transfer coefficent, heat capacity and density data are presented in Table 3. The relative value of iron heat production (q_v = 750 kW/m^3) was set as 1, and then the heat production of other materials could be calculated according to Equation (3), the results are shown in

Table 4. The initial temperature was set at 35 °C, and the temperature distribution at 10000 s was simulated, as shown in Table 5.

Table 4. Relative heat generation of materials

Material	Iron	Copper	Aluminum	Stainless steel	Nichrome	Tungsten	Graphite
Resistivity, $10^{-8}\Omega\cdot m$	9.78	1.75	2.83	40	100	5.56	800
Relative heat generation	1	5.59	3.46	0.23	0.098	1.73	0.012

Table 5. Simulation results for materials

Material	Iron	Copper	Aluminum	Stainless steel	Nichrome	Tungsten	Graphite
t_{max}, °C	766	3889	2549	205.6	104.6	1279	43.97
t_{min}, °C	618	3689	2355	162.5	94.15	1204	42.2
T_a, °C	691	3789	2452	184.1	99.4	1242	43.1
T_d, °C	148	200	194	43.1	10.45	75	1.77

During selection of heater material, the resistivity, temperature coefficient of resistance, melting point, density, heat capacity, thermal conductivity and corrosion resistance were mainly considered, and their respective effect on the heater could be evaluated through temperature distribution. However, the effect of the temperature coefficient of resistance, melting point, thermal expansion coefficient and corrosion resistance could be determined only in real operating conditions.

The centralized pyrolysis temperature of oil shale ranged from 350 to 560 °C, so the temperature of the heater should be controlled at about 760 °C, but generally not below 700 °C. If the temperature was too high, excessive heating would occur near the heating well, which led to the early carbonization and coking of oil shale and harmed the internal wellbore equipment.

The simulation showed that copper and aluminum had the most uniform distribution of temperature. However, the melting point of aluminum is only 660 °C, which does not meet the requirements for heating materials. The melting point of copper is 1083 °C, but its resistivity is extremely low. At the same time, the heating element should be much finer compared with other parts, which leads to lower structure strength.

Tungsten is usually used as a filament material, and the temperature of the incandescent lamp can reach 2000 °C. Among metals, the melting point of tungsten is the highest and its thermal conductivity and electrical conductivity are both very good. The simulation showed that the performance of the tungsten heater was excellent, and the temperature distribution was uniform with a higher bulk temperature. However, the tungsten filament is used

for luminescence only under oxygen-free conditions because at high temperature tungsten is prone to react with various substances. The process of oil shale in-situ development lasts very long, usually for more than 3─5 years. Considering that the heater must be of durable material, the instability of tungsten at high temperature is a serious drawback. Moreover, the price of tungsten is the highest among the six metals under study. Therefore, tungsten is not a good choice as the heating element of the heater.

The simulation temperature of graphite is the lowest and it is the only nonmetallic material among the materials under study. However, graphite has some metalloid properties, such as good thermal conductivity and electric conductivity. Its melting point is above 3000 °C and stability at high temperature good. Another remarkable characteristic of graphite is that the temperature coefficient of resistance is negative below 1200 °C, which means that its resistivity decreases with increasing temperature. The density of graphite is about a quarter that of iron. So, if the graphite heater is sufficiently broad, it also has the advantage of bulk price (price of the unit volume). However, the resistivity of graphite is high and heat power low. Still worse, the mechanical properties of graphite are poorer than those of metals, which hardly meet the requirements for wellbore construction.

The corrosion resistance of nichrome is excellent and its strength at high temperature is high. The major drawbacks of nichrome are its high price and low stability to sulphureous gas. Besides, the resistivity of nichrome as a kind of common resistance wires is too high. Compared with iron and stainless steel, the temperature distribution of nichrome is less uniform, as can be seen from the temperature simulation results.

The physical parameters of iron are superior to those of stainless steel. Its simulation temperature distribution is more uniform and price lower. However, stainless steel has good mechanical and creep properties even at high temperature (1200 °C) and its temperature coefficient of resistance is low. Moreover, the corrosion resistance, strength and hardness as well as welding properties of stainless steel are superior to those of iron.

So, despite some drawbacks, copper, stainless steel and nichrome can all be used as heating materials of the wellbore heater. The heating materials used in the Shell E-ICP project are copper and stainless steel with high Curie point and sulphidization resistance at high temperature, low electric coupling resistance and high creep temperature [16]. Copper was adopted as the heating material of the flange heater by Schniewindt GmbH & Co. KG, Germany. Wang A. M. used the copper wire to produce heat [17]. Nichrome can also be used as a heating element by adjusting the properties.

4.5. Determination of the heater temperature controlling method

The principle of in-situ electric heating technology is utilizing energy generated by resistance heating to heat the oil shale rock. At present, heater temperature is mainly controlled by adjusting voltage and frequency. Since the heating volume of the in-well heater cannot be infinitely increased,

heating rate can be raised by increasing voltage according to the equation $P = U^2/R$ when the temperature field is low. Once the temperature reaches the scheduled value, the optimal heating value can be achieved by decreasing the voltage.

According to the skin effect theory [18] $S = K(1/FC)^{0.5}$, where S refers to the skin effect depth, K refers to the correction factor, and FC refers to frequency. With the increase of FC, S decreases, and the electron transfer outside the conductor surface speeds up. Thus, the AC impedance $Z = KZc(FC)^{0.5}$ increases, which is equivalent to the enlargement of the electric heater resistance value R. As power supply frequency or voltage increases, the load work (thermal energy) also increases. Voltage and frequency can be adjusted, based on the specific properties of oil shale, so that power can also be flexibly regulated. By adopting different frequencies in each test shaft, power factor can be optimized to save electric energy.

When the temperature sensor is installed on the downhole heater [19], the temperature of the heater and downhole fluid can be measured. In the wellhead, the intelligent control cabinet can show whether the downhole heater works trouble-free, and reflect the heating rate of the heater. Furthermore, it realizes the automatic opening of the heater, which can maintain the heater temperature by adjusting heating power.

5. Conclusions

In summary, the temperature distribution of the electric heater was simulated by the PDE Toolbox GUI of MATLAB. The effects of different factors on the temperature distribution of the heater were investigated by orthogonal experiment analysis. The following conclusions can be drawn:

(1) Heat production, density and heat capacity had a significant impact on the heater temperature distribution, while the effect of thermal conductivity could be ignored. The temperature of the heater increased significantly with the increase of heat production and radius of the heater, while higher heat capacity always led to the lower overall temperature of the heater.

(2) The optimal design of the heater is axisymmetrical U-tube and vacuum heating tube.

(3) Copper and stainless steel were proved to be preferred heating materials.

Acknowledgments

The work was performed within the framework of the National Potential Oil and Gas Resources (Exploration, Development and Utilization of Oil Shale Layer) Industry-University-Research-Utilization Cooperative and Innovative Project No OSR-04-07; the Key Laboratory on Deep GeoDrilling

Technology, Ministry of Land and Resources of the China University of Geosciences (Beijing) Project No LSD201207; the Basic Research Funding for Central University Project No 2012098; and the Scientific Development for Drilling Equipment of Deep Continent-Stability Study on Deep Hole and Side Wall Project No SinoProbe-09-05-05.

REFERENCES

1. Liu, Z. J., Dong, Q. S., Ye, S. Q., Zhu, J. W., Guo, W., Li, D. C. et al. The situation of oil shale resources in China. *Journal of Jilin University* (Earth Science Edition), 2006, **36**(6), 870–876 (in Chinese).
2. Li, S. Y., Ma, Y., Qian, J. L. Global oil shale research, development and utilization today and an overview of three oil shale symposiums in 2011. *Sino-Global Energy*, 2012, **17**(2), 8–14 (in Chinese).
3. Liu, D. X., Wang, H. Y., Zheng, D. W., Fang, C. H., Ge, Z. X. World progress of oil shale in-situ exploitation methods. *Natural Gas Industry*, 2009, **29**(5), 128–132 (in Chinese).
4. Kang, Z. Q. *The Pyrolysis Characteristics and In-situ Hot Drive Simulation Research that Exploit Oil-gas of Oil Shale*. A PhD thesis. Taiyuan University of Technology, Taiyuan, 2008 (in Chinese).
5. Rangel-German, E. R., Schembre, J., Sandberg, C., Kovscek, A. R. Electrical-heating-assisted recovery for heavy oil. *J. Petrol. Sci. Eng*., 2004, **45**(3–4), 213–231.
6. Espinosa-Paredes, G., Garcia-Gutierrez, A. Estimation of static formation temperatures in geothermal wells. *Energ. Convers. Manage*., 2003, **44**(8), 1343–1355.
7. Espinosa-Paredes, G., Morales-Diaz, A., Olea-González, U., Ambriz-Garcia, J. J. Application of a proportional-integral control for the estimation of static formation temperatures in oil wells. *Mar. Petrol. Geol*., 2009, **26**(2), 259–268.
8. Espinosa-Paredes, G., Espinosa-Martinez, E. G. A feedback-based inverse heat transfer method to estimate unperturbed temperatures in wellbores. *Energ. Convers. Manage*., 2009, **50**(1), 140–148.
9. Aouizerate, G., Durlofsky, L. J., Samier, P. New models for heater wells in subsurface simulations, with application to the in-situ upgrading of oil shale. *Computat. Geosci*., 2012, **16**(2), 519–533.
10. Burnham, A. K., Day, R. L., Hardy, M. P., Wallman, P. H. AMSO's novel approach to in-situ oil shale recovery. Oil Shale: a solution to the liqud fuel dilemma. *ACS Symposium Series*, 2009, 1032, 149–160.
11. Rodríguez, R., Bashbush, J. L., Rincón, A. Feasibility of using electrical downhole heaters in Faja heavy oil reservoirs. In: *International Thermal Operations and Heavy Oil Symposium, ITOHOS 2008*, 20–23 October 2008, Calgary, Alberta, Canada. Society of Petroleum Engineers, 2008, 2, 823–833.
12. Rodriguez, R., Bashbush, J. L., Rincón, A. Electrical downhole heaters for Faja heavy-oil reservoirs. *J. Petrol. Technol*., 2009, **61**(3), 77–79.
13. Gasbarri, S., Diaz, A., Guzman, M. Evaluation of electric heating on recovery factors in extra heavy oil reservoirs. In: *SPE International Heavy Oil Conference and Exhibition*, 12–14 December 2011, Kuwait City, Kuwait, 91–107.

14. McQueen, G., Parman, D., Williams, H. Enhanced oil recovery of shallow wells with heavy oil: a case study in electro thermal heating of California oil wells. In: *56th Annual Petroleum and Chemical Industry Conference*, Anaheim, Sept. 14–16, 2009, Paper No. PCIC-2009-33, 293–300.
15. Wang, S. P., Liu, D. X., Wang, H. Y., Zhao, Q., Fang, C. H., Zheng, D. W. Current situation and development potential of electric heating process of in-situ oil shale conversion. *Natural Gas Industry*, 2011, **31**(2), 114–118 (in Chinese).
16. Fang, Z. H., Zheng, D. W., Ge, Z. X. *Science and Technology Innovation Herald*, 2010, 36, 110–111 (in Chinese).
17. Wang, A. M., Wang, Z. M. Electric heating hollow rod drive screw pump system. *China Petroleum Machinery (CPM)*, 1998, **26**(3), 36–38 (in Chinese).
18. Peng, R. L., Kang, Y. S., Zha, X., Cao, Z. L., Zhang, W., Yang, S. Z. Improvements of hollow rod for electrical heated oil recovery technology. *Petroleum Geology and Engineering*, 2007, **21**(1), 93–94 (in Chinese).
19. Chen, G. C. Research and application of electrical heating technology for well testing in high pour-point oil wells. *Well Testing*, 2010, **19**(1), 72–74 (in Chinese).

Presented by S. Li
Received May 12, 2013